ACS APPLIED MATERIALS & INTERFACES

Research Article

www.acsami.org

Mussel-Inspired Synthesis of Polydopamine-Functionalized Graphene Hydrogel as Reusable Adsorbents for Water Purification

Hongcai Gao, Yimin Sun, Jiajing Zhou, Rong Xu, and Hongwei Duan*

School of Chemical and Biomedical Engineering, Nanyang Technological University, 70 Nanyang Drive, Singapore 637457

Supporting Information

ABSTRACT: We present a one-step approach to polydopamine-modified graphene hydrogel, with dopamine serving as both reductant and surface functionalization agents. The synthetic method is based on the spontaneous polymerization of dopamine and the self-assembly of graphene nanosheets into porous hydrogel structures. Benefiting from the abundant functional groups of polydopamine and the high specific surface areas of graphene hydrogel with three-dimensional interconnected pores, the prepared material exhibits high adsorption capacities toward a wide spectrum of contaminants, including heavy metals, synthetic dyes, and aromatic pollutants. Importantly, the free-standing graphene hydrogel can be easily removed from water after adsorption process, and can be regenerated by altering the pH values of the solution for adsorbed heavy metals or using low-cost alcohols for synthetic dyes and aromatic molecules.

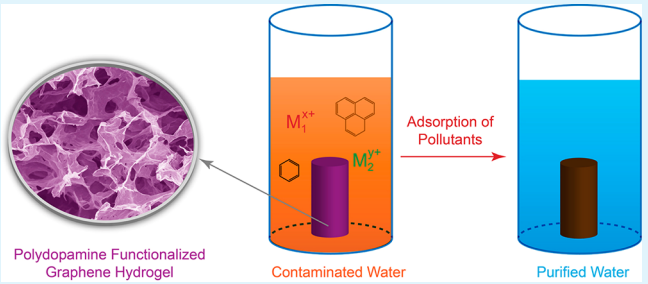

KEYWORDS: *graphene hydrogel, bioinspired coating, polydopamine, water purification, adsorption, heavy metal ions*

1. INTRODUCTION

Recently, tremendous efforts have been devoted to improving the decontamination efficiencies of heavy metals, synthetic dyes, and aromatic pollutants from water because of their detrimental impacts on the environment and human health.[1−3] Technologies actively explored for the removal of these contaminants include chemical precipitation, adsorption, membrane filtration, biological treatment, and photocatalytic degradation.[4,5] Among these methods, adsorption proves to be the most effective and widely used one because of its relatively low cost, ease of operation, and fewer harmful secondary products. However, the traditional adsorbent materials, including activated carbon,[6] silica,[7] metal oxides,[8,9] and polymer resins,[10] suffer from either low adsorption capacities or low efficiencies. The design of nanostructured adsorbents with controlled functionalities offers new possibilities to address these problems because of their high specific surface areas and enhanced active sites.[11] Carbon -based nanomaterials, especially carbon aerogels,[12] carbon nanotubes (CNTs),[13] graphene,[14,15] and their composites,[16] represent a promising type of adsorbents for wastewater treatment, and have demonstrated their potential applications for removal of a range of heavy metals,[17−20] and organic contaminants.[21−27] However, the performance of these carbon nanomaterials is limited by their relatively low density of surface functional groups.[28] Although binding sites can be created by introducing organic functional groups[29,30] or metal oxide nanoparticles[31,32] into these carbon nanomaterials, their complete recovery from water after the adsorption process remains a concern, because the residual nanomaterials if not completely removed are most likely to cause other side-effects in the environment.[33] As a result, an additional step, such as filtration,[34] high-speed centrifugation,[35,36] or magnetic separation,[37,38] is usually necessary to collect these highly dispersed nanomaterials, which increases the operational cost in their practical applications.

To overcome the challenges mentioned above, we report the preparation and application of free-standing graphene hydrogel functionalized with polydopamine for water purification. In our method, dopamine plays dual-functional roles as both the reductant and surface functionalization agents for graphene oxides, while graphene nanosheets are assembled into 3D structures with plenty of interconnected pores and serve as supporting platform to anchor the functional molecules. Belonging to a class of catecholamines with excellent biocompatibility, dopamine can be spontaneously polymerized into polydopamine (PDA) and form adhesive coatings on a wide range of substrates, which was inspired by the properties of adhesive proteins in marine mussels.[39] Besides the extensive research on its self-polymerization, dopamine has also been used as reducing and capping agent for the synthesis of noble metal nanoparticles.[40] The application of the reducing agent of dopamine allows us to prepare functionalized graphene hydrogel under mild conditions and provides greater flexibility than the time-consuming hydrothermal method reported previously.[41,42] Considering these fascinating properties of dopamine, including reduction, self-polymerization, and strong

Received: October 29, 2012
Accepted: December 24, 2012
Published: December 24, 2012

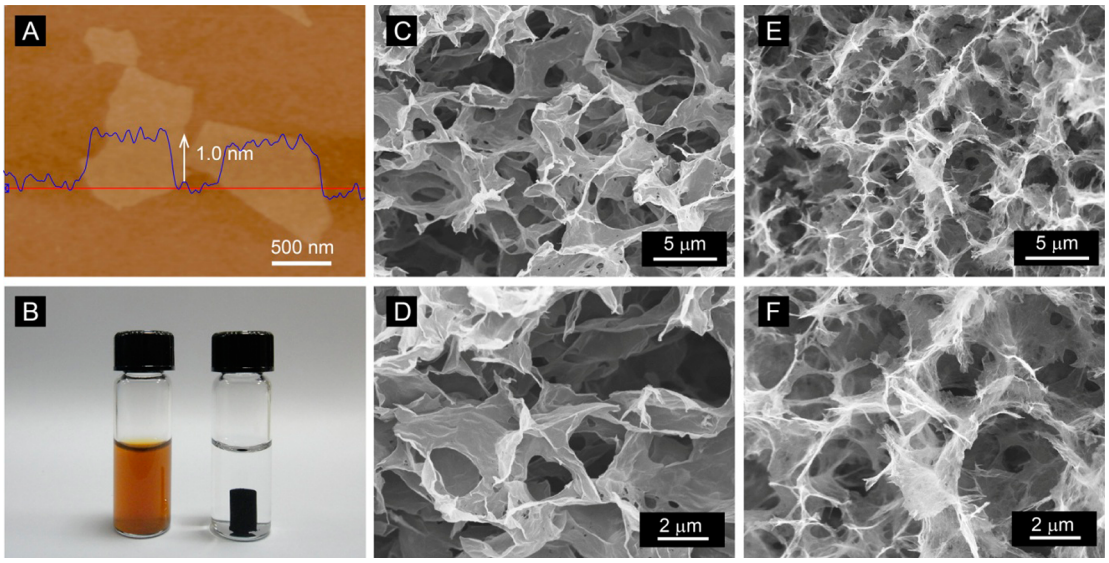

Figure 1. (A) AFM image and height profile of GO spin-coated on silicon wafer. (B) Photograph of GO dispersion mixed with dopamine (left) and the monolithic material of PDA-GH (right). (C, D) SEM images of PDA-GH with low and high magnifications. (E, F) SEM images of HT-GH with low and high magnifications.

adhesion, PDA-modified graphene hydrogel (PDA-GH) was successfully prepared by a one-step procedure in this work. The abundant functional groups especially catechol groups[43] of PDA is expected to be the active sites for heavy metals ions, synthetic dyes and other organic pollutants through electrostatic, bidentate chelating, or hydrogen bonding interactions.[44,45] We found that the resultant PDA-GH exhibits improved adsorption capacities toward different kinds of pollutants compared with pristine graphene hydrogel, and its free-standing nature enables the facile post-treatment process of water. Of equal importance is that the material can be regenerated by low-cost HCl or ethanol to desorb the contaminants and maintains high adsorption capacities after multiple cycles.

2. EXPERIMENTAL SECTION

2.1. Preparation of Samples. Graphene oxides (GO) were synthesized from graphite powder (Sigma-Aldrich) according to the modified Hummers' method.[46,47] Polydopamine functionalized graphene hydrogel (PDA-GH) was prepared by the following procedure using dopamine as the reductant and surface functionalization agent. Typically, dopamine (1.0 mg mL^{-1}) was added into GO aqueous dispersions (2.0 mg mL^{-1}) with pH adjusted to about 7.0, and then the mixture was heated at 60 °C for 6 h without any disturbance to produce PDA-GH. PDA nanoparticles were synthesized from dopamine solution in 10 mM Tris-HCl and purified by centrifugation and washing.[45] Hydrothermally synthesized graphene hydrogel (HT-GH) was also prepared by hydrothermal treatment of 30 mL GO aqueous solution (2.0 mg mL^{-1}) in a 45 mL Teflon-lined autoclave at 180 °C for 12 h.[42] Then, the autoclave was naturally cooled to room temperature and HT-GH was taken out and washed by water. Homogenous dispersions of hydrothermally reduced GO or PDA modified rGO were obtained by using GO solutions with low concentration (0.2 mg mL^{-1}) or under vigorous stirring.

2.2. Materials Characterization. The morphology of the prepared materials was examined by field-emission scanning electron microscope (SEM) (JSM-6701F, JEOL) and atomic force microscopy (AFM) (MFP3D microscope, Asylum Research). The AFM samples were prepared by spin-coating GO dispersion on silicon wafers with a 300 nm SiO_2 top layer and characterized with a silicon cantilever operating in tapping mode. X-ray photoelectron spectroscopy (XPS) were performed on a Kratos-Axis spectrometer with monochromatic Al Kα ($h\nu$ = 1486.71 eV) X-ray radiation (15 kV and 10 mA) and hemispherical electron energy analyzer. All XPS spectra were corrected according to the C 1s line at 284.6 eV. Curve fitting and background subtraction were accomplished using Casa XPS software. Quantachrome Autosorb 6B system was used to characterize the specific surface areas and pore structures of the materials using nitrogen sorption under 77.4 K. The specific surface areas and pore size distributions of the materials were calculated by Brunauer–Emmett–Teller (BET) and Barrett–Joyner–Halenda (BJH) methods, respectively.

2.3. Adsorption Experiments. Batch adsorption experiments were carried out at room temperature to investigate the adsorption behaviors of Pb(II), Cd(II), rhodamine B and p-nitrophenol onto PDA-GH or HT-GH. Typically, PDA-GH or HT-GH (10.0 mg) was placed into 100 mL aqueous solutions containing one of the pollutants with different concentrations in a flask and was shaken in a rotary shaker for a period of time or 12 h to reach adsorption equilibrium. After adsorption, the free-standing PDA-GH and HT-GH were directly removed from the solution. The concentration of metal ions was determined by Prodigy high dispersion inductively coupled plasma (ICP) spectrometer (Teledyne Leeman Laboratories), while the concentration of rhodamine B or *p*-nitrophenol was determined by UV–vis absorption spectra recorded on a Nicolet Evolution 500 Spectrophotometer (Perkin-Elmer). The adsorption capacities of the adsorbents were calculated according to the equation of $q_e = (C_0 - C_e)V/m$, where C_0 and C_e represent the initial and equilibrium concentrations (mg g^{-1}), respectively, where V is the volume of the solutions (mL), and m is the amount of the adsorbents (mg). HCl solution (100 mL, 0.1 M) was used as desorption agent for Pd(II) and Cd(II), and ethanol (100 mL) for rhodamine B and *p*-nitrophenol to regenerate the adsorbents of PDA-GH or HT-GH (10 mg) after shaken for 12 h.

3. RESULTS AND DISCUSSION

3.1. Synthesis and Characterization of Materials. Graphite oxides obtained from Hummer's method were completely exfoliated into single-layered graphene oxides (GO) nanosheets with thickness of about 1.0 nm by a sonication process (Figure 1A).[48,49] After heating the mixtures of GO and dopamine at 60 °C for 6 h, a black cylinder, denoted as polydopamine functionalized graphene hydrogel (PDA-GH), appeared at the bottom of the glass vessel, without any suspended graphene nanosheets or PDA nanoparticles in the

dx.doi.org/10.1021/am302500v | ACS Appl. Mater. Interfaces 2013, 5, 425–432

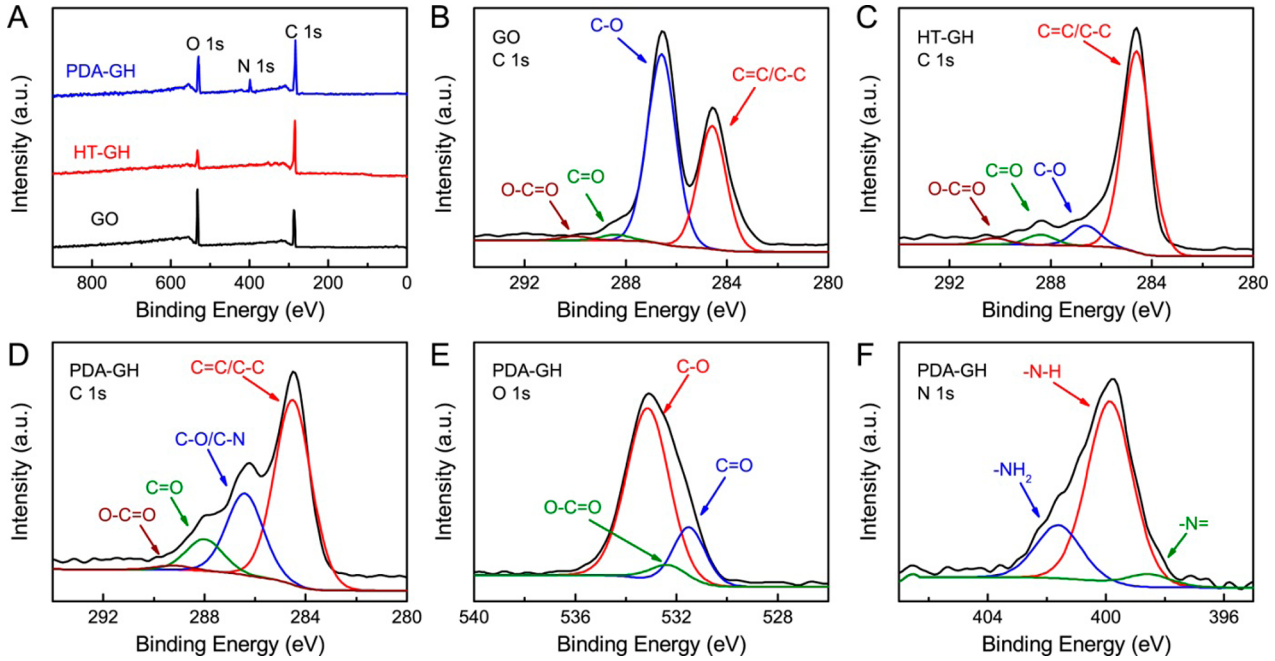

Figure 2. (A) XPS survey spectra of GO, HT-GH, and PDA-GH. High-resolution XPS spectra of C 1s peaks for (B) GO, (C) HT-GH, and (D) PDA-GH. High-resolution XPS spectra of (E) O 1s, and (F) N 1s peaks for PDA-GH.

solution (Figure 1B). We found that the use of GO solution with concentrations higher than 2.0 mg mL^{-1}, and the elimination of any physical disturbance are the crucial factors for the formation of the free-standing PDA-GH. As revealed by SEM images of the freeze-dried PDA-GH, the twisted graphene nanosheets are randomly cross-linked to form a porous structure with wide pore size distributions (Figure 1C and D). The self-assembly of graphene nanosheets into the 3D structures can be attributed to the partial overlapping or coalescence of the flexible reduced GO nanosheets via noncovalent interactions, such as hydrogen bonding, and $\pi-\pi$ interactions.[50,51] For comparison, pristine graphene hydrogel without PDA modification was prepared by hydrothermal reduction of GO solutions (2.0 mg mL^{-1}) at 180 °C for 12 h.[42] A similar porous morphology was observed for hydrothermally synthesized graphene hydrogel (HT-GH) (Figure 1E, F). AFM images reveals that the thickness of hydrothermally reduced GO is about 0.8 nm,[52] whereas the thickness of PDA-modified rGO increases to about 2.0 nm (see Figure S1 in the Supporting Information). The smooth surface of PDA-GH indicates that PDA is uniformly coated on the basal planes of graphene, which may be due to the strong affinity between the dopamine aromatic rings and graphene nanosheets.[53] In addition, PDA-GH and HT-GH possess almost the same specific surface areas, which were measured to be 310.6 and 312.7 m^2 g^{-1}, respectively (see Figure S2 in the Supporting Information).

The compositional change of GO before and after reduction by dopamine or hydrothermal methods was examined by X-ray photoelectron spectroscopy (XPS). The peaks of C 1s and O 1s are observed in GO and HT-GH, while a new peak of N 1s emerges in PDA-GH, which should arise from PDA on the graphene hydrogel (Figure 2A). Deconvolution of the C 1s signal in GO sample shows the presence of C═C/C−C (~284.6 eV), C−O (hydroxyl and epoxy, ~286.5 eV), C═O (carbonyl, ~288.3 eV), and O−C═O (carboxyl, ~290.3 eV) groups (Figure 2B). After hydrothermal reduction, the intensities of the peaks decrease significantly for the heavily oxygenated carbon species, and the peak associated with C═C/C−C (~284.6 eV) becomes dominant (Figure 2C). Although the C1s spectrum of PDA-GH also exhibits the same functionalities of GO, the majority of oxygen-containing groups are removed and some of them may be from PDA (Figure 2D). The O 1s spectrum of PDA-GH peaks is deconvoluted into three components of C═O at 531.1 eV, O−C═O at 532.3 eV, and C−O at 533.3 eV (Figure 2E), which are consistent with those of C 1s. The three components of N 1s peak correspond to amine groups (R−NH_2, 401.7 eV), substituted amines (R-NH-R or indole groups, 399.8 eV), and imino groups (═N-R, 398.5 eV) (Figure 2F). The primary amine group of dopamine was converted to secondary amine, suggesting that dopamine was reacted into indolic compounds during its oxidation by GO and spontaneous polymerization to PDA.[54] The presence of minor amount of primary amine is because of the concurrent existence of noncovalently self-assembled dopamine in the covalent polymerized PDA (see Figure S3 in the Supporting Information).[43] The peak positions and relative amount of N 1s components in PDA-GH resembles those of the synthetic PDA film on silica wafer,[55] further verifying the formation of PDA on graphene hydrogel.

3.2. Adsorption of Heavy Metal Ions. Solution pH is one of the most important factors affecting the surface charges (zeta-potentials) and adsorption characteristics of the adsorbents. The zeta-potentials of both PDA-GH and HT-GH decrease with increasing pH, and the isoelectric points (IEPs) of PDA-GH and HT-GH occur at pH of 3.5 and 4.2 (Figure 3A). Above their corresponding IEPs, the surfaces of the adsorbents are negatively charged due to the ionization of oxygen functional groups. The higher content of oxygen-containing groups of PDA-GH contributes to its more negatively charged surface at the same pH values than HT-GH with minor amount of ionizable groups. As the adsorption process of heavy metal ions is mainly based on electrostatic interactions, it is expected that PDA-GH will possess improved

dx.doi.org/10.1021/am302500v | ACS Appl. Mater. Interfaces 2013, 5, 425−432

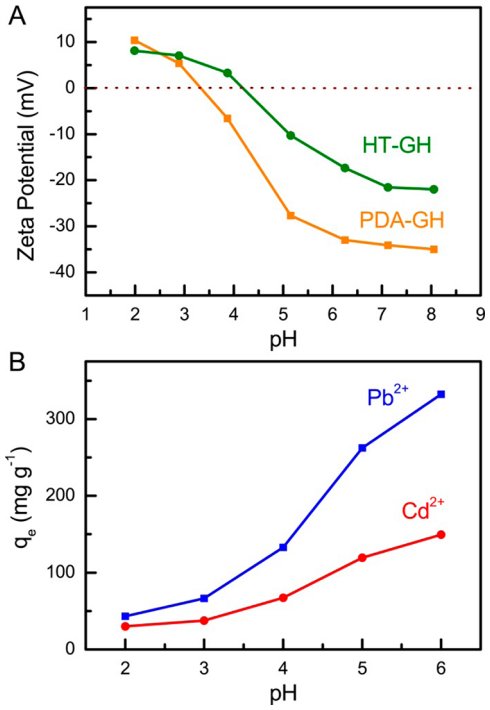

Figure 3. (A) Zeta-potentials of PDA-GH and HT-GH under different pH values. (B) Effects of pH values on the adsorption capacities of Pb(II) and Cd(II) on PDA-GH. Experimental conditions: initial Pb(II) and Cd(II) concentration 500 mg mL^{-1}, temperature 25 °C, and contact time 12 h.

adsorption capacities than HT-GH and the performance of the adsorbents will increase in more alkaline conditions.

To evaluate the effect of pH values on the adsorption of Pb(II) and Cd(II) onto PDA-GH, we conducted batch experiments in a series of solutions with the same initial concentrations and pH values adjusted from 2.0 to 6.0. The adsorbents of PDA-GH were then placed into solutions containing Pb(II) or Cd(II) and gently shaken for 12 h to achieve equilibrium. Afterward, the free-standing PDA-GH was directly removed from the solution, and the concentrations of heavy metal ions were then analyzed. In acidic solutions (pH value lower than 3.0), the species of surface functional groups on PDA-GH were protonized with positively charged surface, and the adsorption capacities of metal ions were low due to the electrostatic repulsion (Figure 3B). With increasing pH values, the surface charges of PDA-GH became more negative, and the adsorption capacities of Pb(II) or Cd(II) dramatically increased in the range of pH values from 3.0 to 6.0. However, if pH values are higher than 6.0, hydrolysis of these two metal ions will occur and result in the formation of metal hydroxide.[56,57] In this condition, the removal mechanism of metal ions will become more complicated, and it will be difficult to distinguish between the adsorption and precipitation of metal ions removed from solutions.

We then compared the adsorption capacities of PDA-GH and HT-GH at pH 6.0 by equilibrium adsorption isotherm studies. The adsorption capacities of the two adsorbents progressively increased with increasing concentrations of metals ions, and finally reached the saturation states (Figure 4A, D). These adsorption data were fitted into the Langmuir and Freundlich isotherm models with the equations given as $q_e = q_{max}K_LC_e/(1 + K_LC_e)$ and $q_e = K_FC_e^{1/n}$, respectively, where q_e is the amount (mg g^{-1}) of metal ions adsorbed at equilibrium, C_e is the equilibrium concentration (mg L^{-1}) of metal ions, K_L and q_{max} (maximum adsorption capacity) are the Langmuir constants of adsorption, and K_F and n are the Freundlich constants of adsorption.[58] The adsorption data could be fitted better with the Langmuir isotherm model, compared with that produced by the Freundlich model (see Table S1 in the Supporting Information), suggesting that the adsorption of metal ions took place at the functional groups or binding sites

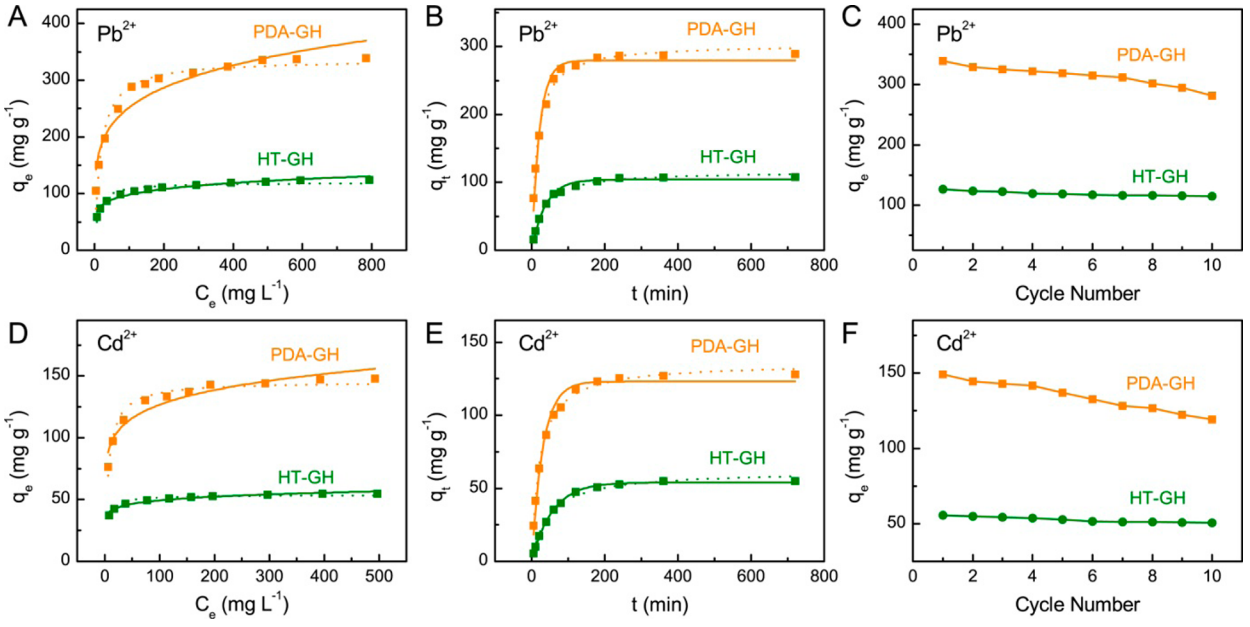

Figure 4. Adsorption behaviors of Pb(II) and Cd(II) on PDA-GH and HT-GH: (A, D) Adsorption isotherm plots and curving fitting by Langmuir (dot line) and Freudlich (solid line) models of Pb(II) and Cd(II) on GH-DA and HT-GH. (B, E) Adsorption kinetic plots and curving fitting by pseudo-first-order (solid line) and pseudo-second-order (dot line) kinetic models of Pb(II) and Cd(II) on GH-DA and HT-GH. (C, F) Adsorption capacities of PDA-GH and HT-GH as a function of repeated adsorption−desorption cycles for the removal of Pb(II) and Cd(II).

dx.doi.org/10.1021/am302500v | ACS Appl. Mater. Interfaces 2013, 5, 425−432

on the surface of adsorbents in a monolayer manner. From the fitting results, we obtained the maximum adsorption capacities of Pb(II) and Cd(II) onto PDA-GH (1:2, w:w) were 336.32 and 145.48 mg g^{-1} (i.e., 1.62 and 1.29 mmol g^{-1}), showing a significant improvement relative to that of HT-GH, PDA, and PDA-GH (0.5:2, w:w) with lower degree of functionalization (see Figure S4 in the Supporting Information). When the mass ratio of PDA:GO increased to 2:2, the strong capping and stabilizing effect of polydopamine can lead to the formation of a black rGO dispersion rather than hydrogels. The relatively higher adsorption capacity of Pb(II) should possibly arise from the higher binding affinity of phenolic and carboxylic groups to Pb (II) compared with Cd(II).[59] The maximum adsorption capacities of PDA-GH for these two metal ions outperform many graphene or CNT-based adsorbents reported previously (see Table S2 in the Supporting Information). More importantly, unlike those suspended adsorbents, our free-standing adsorbents can be easily removed from water after the adsorption process, eliminating the need for time-consuming recovery process, such as filtration, magnetic separation, and high-speed centrifugation.

The adsorption kinetics of Pb(II) or Cd(II) was examined by using the metal ion concentration of 100 mg L^{-1} at pH 6.0, and the samples were collected at different time intervals up to 12 h. The amount of Pb(II) or Cd(II) adsorbed onto HT-GH and PDA-GH increased sharply within the initial 100 min, then rose slowly, and reached equilibrium in 200 min (Figure 4B and E). The pseudofirst order and pseudosecond order kinetic models were employed to fit the experimental data according to the equations of $\ln(q_e - q_t) = \ln(q_e) - k_1 t$ and $t/q_t = 1/k_2 q_e^2 + t/q_e$, respectively, where q_e and q_t are the capacities (mg g^{-1}) of metal ions adsorbed at equilibrium and time t (min), k_1 is the rate constant of pseudofirst order model (min^{-1}), and k_2 is the rate constant of the pseudosecond order model of adsorption (g mg^{-1} min^{-1}).[60] The kinetic model parameters were obtained from fitting the results and presented in Table S3 (see the Supporting Information). On the basis of the value of r^2, it is clear that the pseudo-second-order kinetic model provides a better correlation in contrast to the pseudofirst order model for adsorption of Pb(II) or Cd(II) onto PDA-GH and HT-GH. The pseudo-second-order model is based on the assumption that chemisorption is the rate-determining step,[60] which further confirms the adsorption mechanism in our system. The graphene hydrogel exhibits slightly lower adsorption rates compared with the rGO suspension possibly because of the limited diffusion process of pollutant ions or molecules into pores of the monolithic material (see Figure S5 and Table S4 in the Supporting Information). Nevertheless, as discussed above, the graphene hydrogel can be easily removed after the adsorption process because of its free-standing nature.

The regeneration and reuse of adsorbents is a crucial factor for assessing their potential for practical applications. We found that HCl solutions (0.1 M) can be used as the desorption agent to recover Pd(II) and Cd(II) from the adsorbents of PDA-GH and HT-GH. The decrease of adsorption capacity of PDA-GH could possibly result from reduced stability of the PDA coating in strong acid.[39] However, the adsorption capacities of regenerated PDA-GH were still much higher than those of HT-GH after 10 repeated adsorption and desorption cycles, and more than 80% of its adsorption capacities were retained (Figure 4C, F). Therefore, PDA-GH offers the possibility for easy recycle and reuse for the removal of heavy metal ions.

XPS was employed to analyze the existing forms of Pb(II) or Cd(II) on PDA-GH and the interaction between the metal ions and the adsorbent after adsorption process. The high resolution Pb 4f spectrum can be fitted into two peaks, which appear at 139.0 eV (assigned to Pb $4f_{7/2}$) and 143.9 eV (assigned to Pb $4f_{5/2}$) (Figure 5A). The Pb $4f_{7/2}$ peak at about 139.0 eV, in line

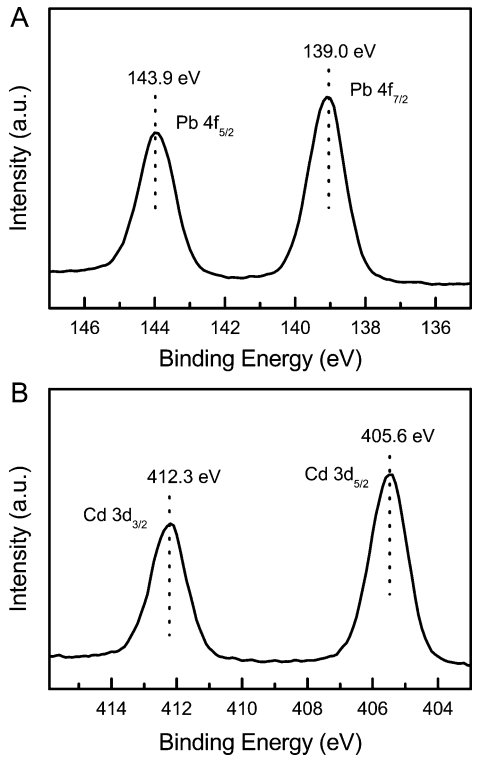

Figure 5. XPS spectra of (A) Pb 4f and (B) Cd 3d after their adsorption on PDA-GH.

with the value reported for PbC_2O_4, can be attributed to the reaction of Pb^{2+} with phenolic and carboxylic groups or their deprotonated form on the surface of PDA-GH.[61] In the hydrolysis material of $Pb(OH)_2$, the Pb $4f_{7/2}$ peak appears at 138.4 eV, indicating the complexation of Pb(II) onto PDA-GH and no precipitation occurs at pH 6.0. The Cd $3d_{5/2}$ spectrum shows a main band centering at 405.6 eV, accompanied by a secondary one at higher binding energy, which can be assigned to Cd $3d_{3/2}$ at 412.3 eV (Figure 5B), whereas the characteristic energy of $Cd(OH)_2$ shows a main band centering at 404.6 eV. These results support that adsorption process involve the interactions of Cd(II) species with the oxygen functional groups on the adsorbents.[62]

3.3. Adsorption of Organic Pollutants. The oxygen functional groups on graphene-based materials plays an important role in controlling the adsorption behavior for organic pollutants and heavy metal ions.[63] Rhodamine B and *p*-nitrophenol with different molecular structures were chosen as model contaminants. The effect of pH on the adsorption performance of PDA-GH was first investigated at different pH values from 2 to 10 (see Figure S6 in the Supporting Information). The adsorption capacity of rhodamine B was maximized at pH 6–7. The adsorption capacity decreases at pH higher than 7 because the deprotonation of amine and carboxylic groups in rhodamine B gives rise to a negatively charged molecule, whose adsorption in turn drops due to the electrostatic repulsion with negative charged PDA-GH

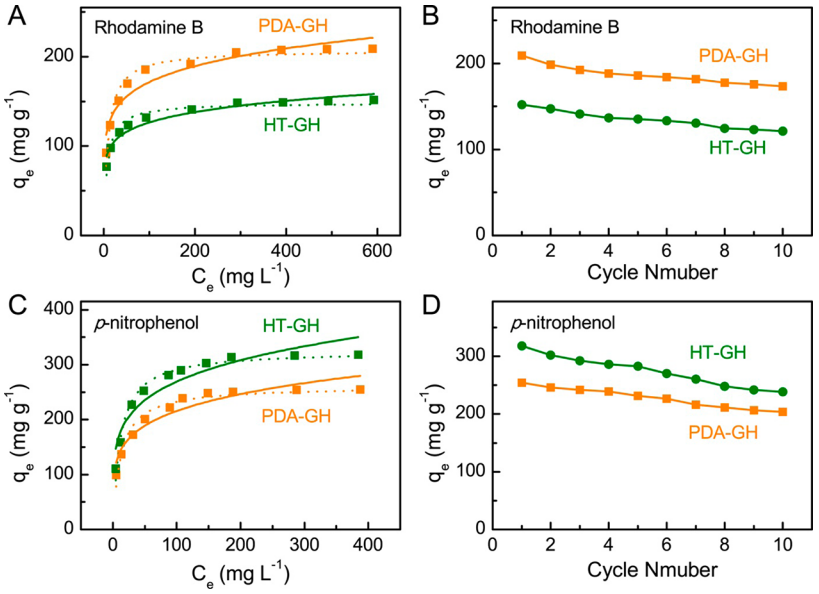

Figure 6. Adsorption behaviors of rhodamine B and *p*-nitrophenol on PDA-GH and HT-GH: (A, C) Adsorption isotherm plots and curving fitting by Langmuir (dot line) and Freundlich (solid line) models of rhodamine B and *p*-nitrophenol on PDA-GH and HT-GH. (B, D) Adsorption capacities of PDA-GH and HT-GH as a function of repeated adsorption−desorption cycles for the removal of rhodamine B and *p*-nitrophenol.

surfaces.[64] In contrast, the adsorption capacity of *p*-nitrophenol remained stable at low pH and decreased when pH rose above 6. At low pH values, *p*-nitrophenol (pK_a = 7.15) is in its neutral form, and $\pi-\pi$ interaction and hydrogen bonding contribute to its adsorption on the substrate. However, at higher pH, the formation of phenolate anions causes electrostatic repulsion with the negatively charged adsorbents, and therefore the adsorption capacity reduces.[65]

The adsorption of rhodamine B and *p*-nitrophenol at different initial concentrations was studied at room temperature with adsorption time of 12 h. The rhodamine B solution which initially displays pink color became colorless after the treatment by PDA-GH. The adsorption data could also be fitted with both of the isotherm models mentioned above and the Langmuir isotherm model presented a better result (Figure 6A, C). The adsorption constants evaluated from the isotherms are listed in Table S5 (see the Supporting Information). PDA-GH processes a higher maximum adsorption capacity for rhodamine B (207.06 mg g^{-1} or 0.43 mmol g^{-1}) than HT-GH (148.41 mg g^{-1} or 0.31 mmol g^{-1}). The chemical structure of rhodamine B has cationic atoms (N^+), which are favorable for their adsorption on PDA-GH with larger amount of negatively charged oxygen functional groups through electrostatic interactions.[66] However, HT-GH exhibits higher adsorption capacity for *p*-nitrophenol (324.89 mg g^{-1} or 2.34 mmol g^{-1}) compared with PDA-GH (260.38 mg g^{-1} or 1.15 mmol g^{-1}). The relatively lower adsorption capacity of rhodamine B onto these two adsorbents compared with *p*-nitrophenol can be explained by the larger molecular size of rhodamine B and the unavailability of small pores to the larger dye molecule.[67] The mechanism of *p*-nitrophenol adsorption is dominated by $\pi-\pi$ interactions.[68,69] We reason that introducing the hydrophilic PDA coating can weaken the $\pi-\pi$ interaction between the aromatic ring of *p*-nitrophenol and the graphitic structure of graphene hydrogel, and as a result, PDA-GH exhibits lower uptake of *p*-nitrophenol than HT-GH. To regenerate the adsorbents, we can use ethanol as the desorption agent, and PDA-GH and HT-GH exhibited high adsorption capacities for these two organic pollutants without significant decline after 10 repeated adsorption and desorption treatments (Figure 6B, D).

4. CONCLUSION

We have demonstrated a one-step method to prepare PDA functionalized graphene hydrogel and found that the adsorption capacity of PDA-GH for different kinds of pollutants was greatly enhanced in comparison with HT-GH. The formation of free-standing graphene hydrogel with sufficient functionalities effectively addressed the problems associated with carbon nanomaterials in water purification, such as low adsorption capacity, complicated recovery process, and potential side effects due to the residual adsorbents in water. Importantly, PDA-GH can be easily regenerated by low-cost reagents, and exhibited high adsorption capacity after multiple adsorption−desorption cycles. Taken together, PDA-GH is of great potential as a new class of freestanding adsorbent for water purification.

■ ASSOCIATED CONTENT

Supporting Information

Additional figures and tables. This material is available free of charge via the Internet at http://pubs.acs.org.

■ AUTHOR INFORMATION

Corresponding Author

*E-mail: hduan@ntu.edu.sg.

Notes

The authors declare no competing financial interest.

■ ACKNOWLEDGMENTS

H.D. thanks the program of Nanyang Assistant Professorship for financial support. H.G. is a recipient of graduate research scholarship supported by Nanyang Technological University, Singapore. This work is also supported by the INSIST program at Nanyang Technological University.

REFERENCES

(1) He, F.; Wang, W.; Moon, J. W.; Howe, J.; Pierce, E. M.; Liang, L. Y. *ACS Appl. Mater. Interfaces* **2012**, *4*, 4373−4379.
(2) Cao, C. Y.; Qu, J.; Yan, W. S.; Zhu, J. F.; Wu, Z. Y.; Song, W. G. *Langmuir* **2012**, *28*, 4573−4579.
(3) Warner, C. L.; Chouyyok, W.; Mackie, K. E.; Neiner, D.; Saraf, L. V.; Droubay, T. C.; Warner, M. G.; Addleman, R. S. *Langmuir* **2012**, *28*, 3931−3937.
(4) Khin, M. M.; Nair, A. S.; Babu, V. J.; Murugan, R.; Ramakrishna, S. *Energy Environ. Sci* **2012**, *5*, 8075−8109.
(5) Fu, F. L.; Wang, Q. *J. Environ. Manag.* **2011**, *92*, 407−418.
(6) Gupta, V. K.; Carrott, P. J. M.; Ribeiro Carrott, M. M. L.; Suhas. *Crit. Rev. Environ. Sci. Technol.* **2009**, *39*, 783−842.
(7) Repo, E.; Warchol, J. K.; Bhatnagar, A.; Sillanpaa, M. *J. Colloid Interface Sci.* **2011**, *358*, 261−267.
(8) Cao, C. Y.; Qu, J.; Wei, F.; Liu, H.; Song, W. G. *ACS Appl. Mater. Interfaces* **2012**, *4*, 4283−4287.
(9) Zhai, T.; Xie, S. L.; Lu, X. H.; Xiang, L.; Yu, M. H.; Li, W.; Liang, C. L.; Mo, C. H.; Zeng, F.; Luan, T. G.; Tong, Y. X. *Langmuir* **2012**, *28*, 11078−11085.
(10) Zhang, Y.; Li, Y. F.; Yang, L. Q.; Ma, X. J.; Wang, L. Y.; Ye, Z. F. *J. Hazard. Mater.* **2010**, *178*, 1046−1054.
(11) Sharma, Y. C.; Srivastava, V.; Singh, V. K.; Kaul, S. N.; Weng, C. H. *Environ. Technol.* **2009**, *30*, 583−609.
(12) Ling, S. K.; Tian, H. Y.; Wang, S. B.; Rufford, T.; Zhu, Z. H.; Buckley, C. E. *J. Colloid Interface Sci.* **2011**, *357*, 157−162.
(13) Wang, S. B.; Ng, C. W.; Wang, W. T.; Li, Q.; Li, L. Q. *J. Chem. Eng. Data* **2012**, *57*, 1563−1569.
(14) Zhao, G. X.; Wen, T.; Chen, C. L.; Wang, X. K. *RSC Adv* **2012**, *2*, 9286−9303.
(15) Bradder, P.; Ling, S. K.; Wang, S. B.; Liu, S. M. *J. Chem. Eng. Data* **2011**, *56*, 138−141.
(16) Yao, Y. J.; Miao, S. D.; Liu, S. Z.; Ma, L. P.; Sun, H. Q.; Wang, S. B. *Chem. Eng. J.* **2012**, *184*, 326−332.
(17) Zhao, G. X.; Li, J. X.; Ren, X. M.; Chen, C. L.; Wang, X. K. *Environ. Sci. Technol.* **2011**, *45*, 10454−10462.
(18) Lin, D. H.; Tian, X. L.; Li, T. T.; Zhang, Z. Y.; He, X.; Xing, B. S. *Environ. Pollut.* **2012**, *167*, 138−147.
(19) Rao, G. P.; Lu, C.; Su, F. *Sep. Purif. Technol.* **2007**, *58*, 224−231.
(20) Cong, H. P.; Ren, X. C.; Wang, P.; Yu, S. H. *ACS Nano* **2012**, *6*, 2693−2703.
(21) Gupta, S. S.; Sreeprasad, T. S.; Maliyekkal, S. M.; Das, S. K.; Pradeep, T. *ACS Appl. Mater. Interfaces* **2012**, *4*, 4156−4163.
(22) Gao, W.; Majumder, M.; Alemany, L. B.; Narayanan, T. N.; Ibarra, M. A.; Pradhan, B. K.; Ajayan, P. M. *ACS Appl. Mater. Interfaces* **2011**, *3*, 1821−1826.
(23) Bi, H.; Xie, X.; Yin, K.; Zhou, Y.; Wan, S.; He, L.; Xu, F.; Banhart, F.; Sun, L.; Ruoff, R. S. *Adv. Funct. Mater.* **2012**, *22*, 4421−4425.
(24) Liu, F.; Chung, S.; Oh, G.; Seo, T. S. *ACS Appl. Mater. Interfaces* **2012**, *4*, 922−927.
(25) Xu, J.; Wang, L.; Zhu, Y. F. *Langmuir* **2012**, *28*, 8418−8425.
(26) Sui, Z. Y.; Meng, Q. H.; Zhang, X. T.; Ma, R.; Cao, B. *J. Mater. Chem.* **2012**, *22*, 8767−8771.
(27) Maliyekkal, S. M.; Sreeprasad, T. S.; Krishnan, D.; Kouser, S.; Mishra, A. K.; Waghmare, U. V.; Pradeep, T. *Small* **2012**, DOI: 10.1002/smll.201201125.
(28) Mauter, M. S.; Elimelech, M. *Environ. Sci. Technol.* **2008**, *42*, 5843−5859.
(29) Madadrang, C. J.; Kim, H. Y.; Gao, G. H.; Wang, N.; Zhu, J.; Feng, H.; Gorring, M.; Kasner, M. L.; Hou, S. F. *ACS Appl. Mater. Interfaces* **2012**, *4*, 1186−1193.
(30) Song, H. J.; Hao, L. Y.; Tian, Y. F.; Wan, X. Y.; Zhang, L. C.; Lv, Y. *ChemPlusChem* **2012**, *77*, 379−386.
(31) Zhu, J. H.; Wei, S. Y.; Gu, H. B.; Rapole, S. B.; Wang, Q.; Luo, Z. P.; Haldolaarachchige, N.; Young, D. P.; Guo, Z. H. *Environ. Sci. Technol.* **2012**, *46*, 977−985.
(32) Wang, J. F.; Tsuzuki, T.; Tang, B.; Hou, X. L.; Sun, L.; Wang, X. G. *ACS Appl. Mater. Interfaces* **2012**, *4*, 3084−3090.
(33) Liao, K. H.; Lin, Y. S.; Macosko, C. W.; Haynes, C. L. *ACS Appl. Mater. Interfaces* **2011**, *3*, 2607−2615.
(34) Huang, Z. H.; Zheng, X. Y.; Lv, W.; Wang, M.; Yang, Q. H.; Kang, F. Y. *Langmuir* **2011**, *27*, 7558−7562.
(35) Ramesha, G. K.; Kumara, A. V.; Muralidhara, H. B.; Sampath, S. *J. Colloid Interface Sci.* **2011**, *361*, 270−277.
(36) Yang, S. T.; Chen, S.; Chang, Y. L.; Cao, A. N.; Liu, Y. F.; Wang, H. F. *J. Colloid Interface Sci.* **2011**, *359*, 24−29.
(37) Xie, G. Q.; Xi, P. X.; Liu, H. Y.; Chen, F. J.; Huang, L.; Shi, Y. J.; Hou, F. P.; Zeng, Z. Z.; Shao, C. W.; Wang, J. *J. Mater. Chem.* **2012**, *22*, 1033−1039.
(38) Chandra, V.; Park, J.; Chun, Y.; Lee, J. W.; Hwang, I. C.; Kim, K. S. *ACS Nano* **2010**, *4*, 3979−3986.
(39) Lee, H.; Dellatore, S. M.; Miller, W. M.; Messersmith, P. B. *Science* **2007**, *318*, 426−430.
(40) Baron, R.; Zayats, M.; Willner, I. *Anal. Chem.* **2005**, *77*, 1566−1571.
(41) Liang, H. W.; Guan, Q. F.; Chen, L. F.; Zhu, Z.; Zhang, W. J.; Yu, S. H. *Angew. Chem., Int. Ed.* **2012**, *51*, 5101−5105.
(42) Xu, Y. X.; Sheng, K. X.; Li, C.; Shi, G. Q. *ACS Nano* **2010**, *4*, 4324−4330.
(43) Hong, S.; Na, Y. S.; Choi, S.; Song, I. T.; Kim, W. Y.; Lee, H. *Adv. Funct. Mater.* **2012**, *22*, 4711−4717.
(44) Ye, Q.; Zhou, F.; Liu, W. M. *Chem. Soc. Rev.* **2011**, *40*, 4244−4258.
(45) Farnad, N.; Farhadi, K.; Voelcker, N. H. *Water Air Soil Pollut.* **2012**, *223*, 3535−3544.
(46) Hummers, W. S.; Offeman, R. E. *J. Am. Chem. Soc.* **1958**, *80*, 1339−1339.
(47) Gao, H. C.; Xiao, F.; Ching, C. B.; Duan, H. W. *ACS Appl. Mater. Interfaces* **2011**, *3*, 3049−3057.
(48) Stankovich, S.; Piner, R. D.; Nguyen, S. T.; Ruoff, R. S. *Carbon* **2006**, *44*, 3342−3347.
(49) Xiao, F.; Song, J. B.; Gao, H. C.; Zan, X. L.; Xu, R.; Duan, H. W. *ACS Nano* **2012**, *6*, 100−110.
(50) Bai, H.; Li, C.; Wang, X. L.; Shi, G. Q. *J. Phys. Chem. C* **2011**, *115*, 5545−5551.
(51) Gao, H. C.; Xiao, F.; Ching, C. B.; Duan, H. W. *ACS Appl. Mater. Interfaces* **2012**, *4*, 2801−2810.
(52) Gao, H. C.; Wang, Y. X.; Xiao, F.; Ching, C. B.; Duan, H. W. *J. Phys. Chem. C* **2012**, *116*, 7719−7725.
(53) Kang, S. M.; Park, S.; Kim, D.; Park, S. Y.; Ruoff, R. S.; Lee, H. *Adv. Funct. Mater.* **2011**, *21*, 108−112.
(54) Clark, M. B.; Gardella, J. A.; Schultz, T. M.; Patil, D. G.; Salvati, L. *Anal. Chem.* **1990**, *62*, 949−956.
(55) Bernsmann, F.; Ponche, A.; Ringwald, C.; Hemmerle, J.; Raya, J.; Bechinger, B.; Voegel, J. C.; Schaaf, P.; Ball, V. *J. Phys. Chem. C* **2009**, *113*, 8234−8242.
(56) Lai, C. H.; Chen, C. Y.; Wei, B. L.; Yeh, S. H. *Water Res.* **2002**, *36*, 4943−4950.
(57) Weng, C. H. *J. Colloid Interface Sci.* **2004**, *272*, 262−270.
(58) Gerente, C.; Lee, V. K. C.; Le Cloirec, P.; McKay, G. *Crit. Rev. Environ. Sci. Technol.* **2007**, *37*, 41−127.
(59) Kinniburgh, D. G.; Milne, C. J.; Benedetti, M. F.; Pinheiro, J. P.; Filius, J.; Koopal, L. K.; Van Riemsdijk, W. H. *Environ. Sci. Technol.* **1996**, *30*, 1687−1698.
(60) Ho, Y. S.; Ng, J. C. Y.; McKay, G. *Sep. Purif. Methods* **2000**, *29*, 189−232.
(61) Yu, X. Y.; Luo, T.; Zhang, Y. X.; Jia, Y.; Zhu, B. J.; Fu, X. C.; Liu, J. H.; Huang, X. J. *ACS Appl. Mater. Interfaces* **2011**, *3*, 2585−2593.
(62) Gao, Z. M.; Bandosz, T. J.; Zhao, Z. B.; Han, M.; Liang, C. H.; Qiu, J. S. *Langmuir* **2008**, *24*, 11701−11710.
(63) Yang, X.; Chen, C. L.; Li, J. X.; Zhao, G. X.; Ren, X. M.; Wang, X. K. *RSC Adv.* **2012**, *2*, 8821−8826.
(64) Sun, H. M.; Cao, L. Y.; Lu, L. H. *Nano Res.* **2011**, *4*, 550−562.
(65) Tang, D. Y.; Zheng, Z.; Lin, K.; Luan, J. F.; Zhang, J. B. *J. Hazard. Mater.* **2007**, *143*, 49−56.
(66) Pereira, M. F. R.; Soares, S. F.; Orfao, J. J. M.; Figueiredo, J. L. *Carbon* **2003**, *41*, 811−821.

(67) Attia, A. A.; Girgis, B. S.; Khedr, S. A. *J. Chem. Technol. Biotechnol.* **2003**, *78*, 611−619.
(68) Arasteh, R.; Masoumi, M.; Rashidi, A. M.; Moradi, L.; Samimi, V.; Mostafavi, S. T. *Appl. Surf. Sci.* **2010**, *256*, 4447−4455.
(69) Zhao, G. X.; Jiang, L.; He, Y. D.; Li, J. X.; Dong, H. L.; Wang, X. K.; Hu, W. P. *Adv. Mater.* **2011**, *23*, 3959−3963.